**Spatial Scale and the Spread of a Fungal Pathogen of Gypsy Moth**

Greg Dwyer; Joseph S. Elkinton; Ann E. Hajek

*American Naturalist*, Vol. 152, No. 3 (Sep., 1998), 485-494.

Stable URL:
http://links.jstor.org/sici?sici=0003-0147%28199809%29152%3A3%3C485%3ASSATSO%3E2.0.CO%3B2-P

*American Naturalist* is currently published by The University of Chicago Press.

# Spatial Scale and the Spread of a Fungal Pathogen of Gypsy Moth

Greg Dwyer,[1,*] Joseph S. Elkinton,[1] and Ann E. Hajek[2]

1. Department of Entomology, University of Massachusetts, Amherst, Massachusetts 01003-2410;
2. Department of Entomology, Cornell University, Ithaca, New York 14853

*Submitted October 20, 1997; Accepted March 20, 1998*

*Keywords:* spatial scale, disease transmission, mathematical model, *Entomophaga maimaiga*.

For reasons of logistics, most ecological studies focus on small spatial scales, in study plots that typically range in size from 0.1 $m^2$ to 1 ha (Kareiva and Andersen 1990), yet many interesting ecological phenomena occur at scales that range from square kilometers to the size of the globe (Mooney and Drake 1986; Vitousek 1994). If small-scale studies are to have relevance for large-scale phenomena, the ability to extrapolate between scales is critical. One way of extrapolating between spatial scales is through the use of mathematical models that incorporate explicit spatial structure. In this note, we use data from a field experiment on the spatial spread of an insect pathogen (Hajek et al. 1996) to try to understand the spread of the pathogen over a large area of central New York and Pennsylvania (Elkinton et al. 1991).

The disease in our study is the fungal pathogen *Entomophaga maimaiga* that infects larvae of the gypsy moth *Lymantria dispar*. This pathogen was first introduced into North America between 1910 and 1911 as a biological control agent to be used against gypsy moth (Hajek et al. 1995). For unknown reasons, it then apparently disappeared until it caused a massive epidemic among northeastern gypsy moth populations in 1989 (Hajek et al. 1990*a*). The large-scale data that we use track the spread of the disease across central New York and Pennsylvania from 1989 to 1990 (Elkinton et al. 1991). The disease was subsequently introduced into Virginia in 1991 by artificial means (Hajek et al. 1996), which afforded the opportunity to observe the spread of the disease in the early stages of introduction. In the field experiment, the pathogen spread no more than 300 m in a single season, but in the natural epidemic, it spread more than 100 km in a single season. The question that we ask is, What explains the differences in the rate of spread of the disease at the two spatial scales?

Our approach is to use a spatial mathematical model that is part of a long tradition of spatial modeling in ecology, dating from the work of Fisher (Murray 1989). In most such models the population of the invading species forms a wavefront that moves across the landscape at a constant speed (fig. 1), and for an interspecific interaction the speed of the wavefront depends on the densities of both interacting species. This means that small increases in the density of the host or the pathogen can lead to large increases in the speed of the wavefront of disease, and the long-term rate of spread of the disease will be higher than the initial rate of spread. We therefore use the model to ask whether the higher rate of spread of the disease at the larger scale may have been due to a combination of higher densities of both host and pathogen at the larger scale. The density of the host in the region in which large-scale spread occurred was higher than it was where the pathogen was experimentally introduced, and pathogen densities were higher in the region of large-scale spread because the disease had built up to high levels in the previous season's epidemic. Our question is then, What fraction of the higher rate at the regional scale can be explained by the wavefront of disease reaching its long-term spread rate in a higher density population? In other words, to what extent is the higher rate at the larger scale due simply to density effects, rather than to a different mechanism of spread at the larger scale?

## Methods and Results

### *Natural History of Gypsy Moth and Its Fungal Pathogen*

The gypsy moth was introduced into the northeastern United States in 1868 and is a significant forest pest during its episodic outbreaks (Campbell 1981). Outbreaks historically have been terminated by epidemics of a nuclear polyhedrosis virus (Elkinton and Liebhold 1990),

* Present address: Department of Ecology and Evolution, University of Chicago, 1101 East 57 Street, Chicago, Illinois 60637; E-mail: gdwyer@midway.uchicago.edu.

Am Nat. 1998. Vol. 152, pp. 485–494. 

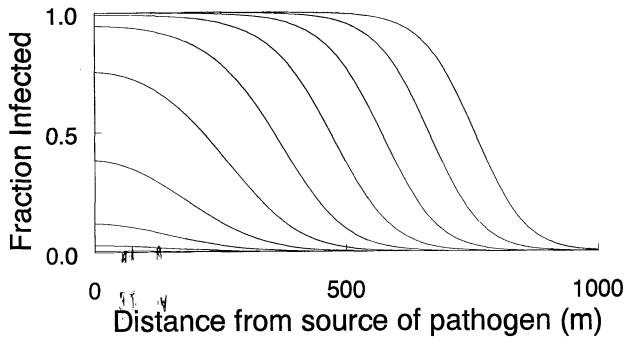


**Figure 1:** Behavior of the model equations (1)–(3) over the long term. Moving from left to right, successive curves show the wave of infection at 1-wk intervals. As time passes, the initially low rates of infection at the point of introduction of the disease increase to high levels, and the disease forms a wave front of infection that moves over the landscape with constant shape and velocity. Note that the rate of advance of the disease is at first extremely low but builds up to a rapid rate as infection rates increase. The parameters here were taken from the best fit of the model to data from the Holloway Gap plot (fig. 2).

but since the reappearance of *Entomophaga maimaiga* in 1989, high density populations in northeastern North America have been associated with high levels of *E. maimaiga* infection. Since it reappeared in 1989, *E. maimaiga* has continued to spread across the range of gypsy moth in North America (Hajek et al. 1995, 1996).

*Entomophaga maimaiga* is a pathogen of larvae that kills its host in about 4–7 d at 20°C (Hajek et al. 1993). After the death of the host, the fungus produces one of two types of spores, depending on the instar of the host that it infected. Overwintering resting spores (azygospores) are produced by cadavers of later instar larvae and are leached from cadavers into soil and onto tree bark where they lie dormant until spring, forming a reservoir for the pathogen. Relatively short-lived conidia are actively ejected from cadavers of earlier instars and some later instars, causing infections during the same season and generating epidemics. Because aerial sampling has often documented high levels of airborne conidia within forest canopies, and because experiments have demonstrated that these airborne conidia are alive and infective (A. E. Hajek, unpublished data), airborne conidia are believed to be the dispersal phase of the fungus. Although *E. maimaiga* is directly transmitted, unlike many insect viruses that cause infection only after being consumed (Fuxa and Tanada 1987; Tanada and Kaya 1993), *E. maimaiga* causes infection by direct penetration of the larval integument.

## *The Data Sets*

As we described earlier, our concern is with differences in the rate of spread of the disease at two different spatial scales.

*Moderate Scale Experimental Data.* The moderate-scale data come from efforts to introduce *E. maimaiga* into gypsy moth populations in Virginia in 1991. Because the details of the experimental protocol are described elsewhere (Hajek et al. 1996), here we give only a summary of the experiment. Soil contaminated with *E. maimaiga* resting spores was placed in the center of nine geographically separate plots. Gypsy moth densities in these plots were at the lower end of outbreaking densities, as shown by standard methods of estimating egg mass densities (Woods et al. 1991; see fig. 2). The spatial spread of the disease was measured at the end of the larval period (late June, early July) by collections of cadavers at intervals of 50–100 m from the release point, following two transects that were laid out in haphazard directions relative to the central release point in each plot. The data that we use are the fraction of cadavers that were infected with *E. maimaiga*. As figure 2 shows, the disease spread as far as 275 m in the course of the season, and this is our definition of a moderate spatial scale.

*Regional Scale Spread Data.* The regional scale data come from observations of the 1991 spread of *E. maimaiga* across New York and Pennsylvania. The 1989 epidemic caused high mortality in gypsy moth populations throughout New England, and, in 1990, the pathogen was recovered in central New York and Pennsylvania where it had not been found in 1989 (Elkinton et al. 1991). The vastness of this regional scale means that we do not have the precise density information that we have at the experimental scale; however, the extensive defoliation that occurred throughout this region at that time (Gypsy Moth News 1990) suggests that gypsy moths were at outbreak densities, or in the vicinity of 20,000 egg masses $ha^{-1}$, at the beginning of each season.

We used the regional data to quantify the spread of *E. maimaiga* at a large scale. To do this, we calculated the distance that the fungus spread between 13 pairs of points, where each point was a location at the western limit of fungus spread in either 1989 or 1990. Pairs of points were selected by first picking a 1989 point and then finding the closest 1990 point to the 1989 point. As our measure of the regional fungus spread rate, we then used the average of the resulting 13 distances, which gave 121.5 km (SE = 14.3) as the spread rate of the disease from the end of one gypsy moth larval period to the end of the next.

## *A Model of* E. maimaiga *Spread*

In order to extrapolate from the moderate scale of the experimental release of the pathogen to the large scale of the regional spread, we fit a simple mathematical model

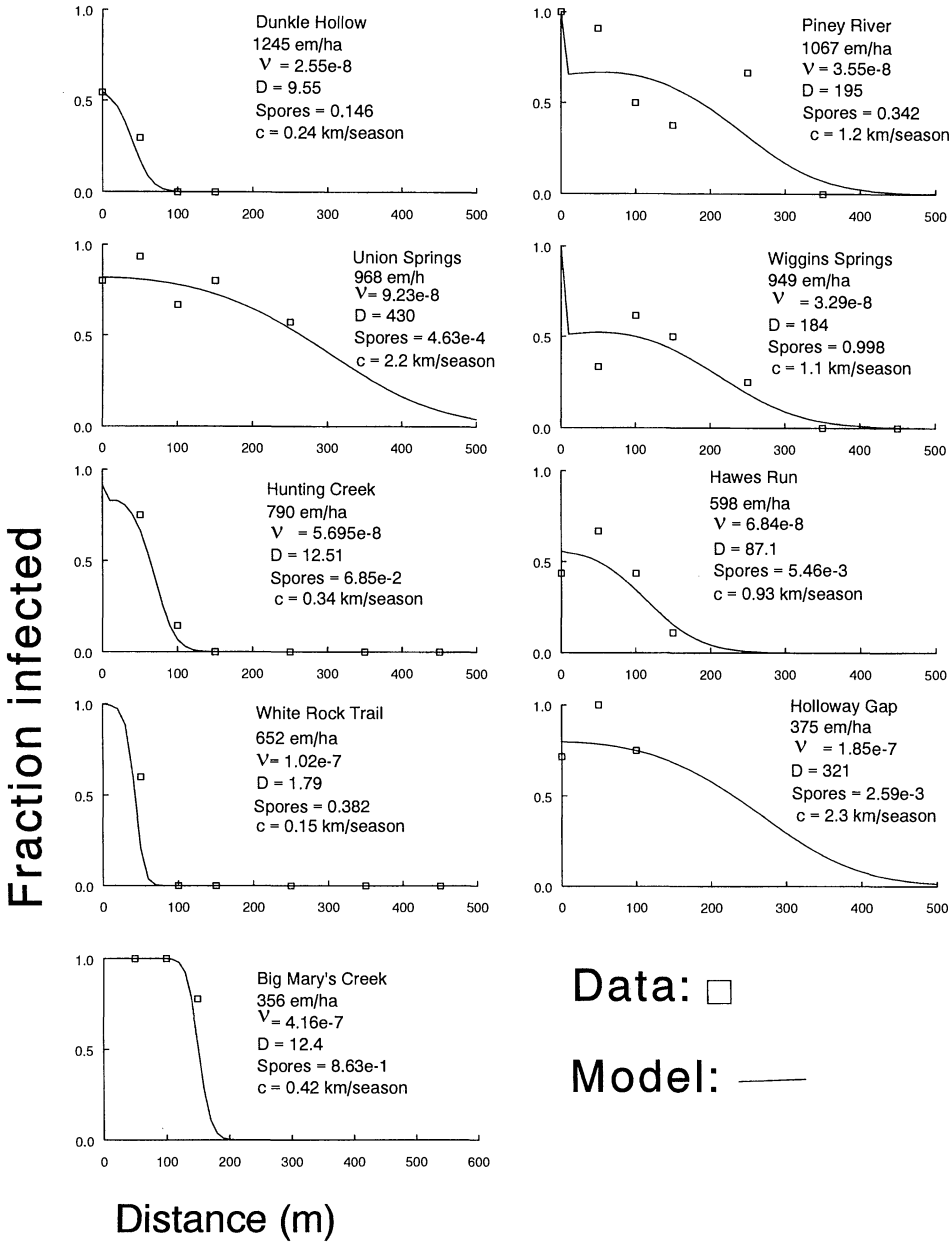


**Figure 2:** Best fit of the model equations (1)–(3) to data from nine experimental release plots. The horizontal axes indicate the distance from the point at which the fungus was released. The data show the cumulative percentage of cadavers at each point that were infected with the disease. *em/ha* = egg masses $ha^{-1}$; $\nu$ = the conidial transmission coefficient, in units of $m^{-2}\ d^{-1}$; $D$ = the conidial diffusion coefficient, in units of $m^2\ d^{-1}$; *spores* indicates the resting spore force of infection, $\nu_R R$, in units of $d^{-1}$; $c$ = the long-term rate of spread of the disease calculated from the set of parameters listed for each plot, in units of km $season^{-1}$.

to the experimental data and then attempted to predict the large-scale spread rate using the model. The model is

$$\frac{\partial S}{\partial t} = -(\nu_C C + \nu_R R)S, \tag{1}$$

$$\frac{\partial I}{\partial t} = (\nu_C C + \nu_R R)S - \alpha I, \tag{2}$$

and

$$\frac{\partial C}{\partial t} = \lambda I - \mu C + D\frac{\partial^2 C}{\partial x^2}, \tag{3}$$

where $S$ is the density of healthy larvae, $I$ is the density of infected larvae, $C$ is the density of conidia, $R$ is the density of resting spores, $\nu_C$ is the transmission rate of

conidia, $\nu_R$ is the transmission rate of resting spores, $\alpha$ is the death rate of infected larvae, $\lambda$ is the rate at which infected larvae produce conidia, $\mu$ is the breakdown rate of conidia, and $D$ is the dispersal rate of conidia. This is a standard insect-pathogen model (Anderson and May 1994), except that it keeps track of the spread of the disease in both time and space. We can therefore use the model to track the course of the epidemic across the landscape. The epidemic in the model begins when resting spores are introduced into the center of the landscape; field observations suggest that the population of resting spores is roughly constant for the rest of the season (A. E. Hajek, unpublished data). The resting spores infect larvae that then infect additional larvae by producing conidia. Resting spores are only found on the ground, however, and consequently cannot infect second and third instars that spend all of their time in the canopy (fourth and fifth instars spend the day on or near the ground; Elkinton and Liebhold 1990). Also, transmission from resting spores tends to be very low among late fifth and sixth instar larvae. We allow for these patterns in the model by not allowing infections from resting spores in the third and fourth weeks of the season (out of a total of 8 wk), when second and third instars are normally present, and in the last week, when late fifth and sixth instars are present.

Most fungal infections occur after larvae finish ballooning, by which time the larval dispersal rate is very low relative to the dispersal of conidia (Liebhold et al. 1986). Model simulations that we do not show here demonstrated that larval dispersal by crawling has no effect on the spread rate of the pathogen. We therefore assume that only conidia disperse.

We assume that dispersal of conidia is random, so that dispersal can be modeled as though conidia are particles of a diffusing gas. In reality, wind dispersal of microscopic particles like *E. maimaiga* conidia is a complex process (Pasquill and Smith 1983; Okubo and Levin 1989). Models that allow for these processes, however, require as a minimum four-dimensional wind speed data (three spatial dimensions plus time) and are consequently too data intensive for what we are attempting here. Instead we assume in equations (1)–(3) that wind directionality and speed vary rapidly enough so as to be essentially random.

Figure 1 illustrates the kind of long-term behavior that equations (1)–(3) show when the disease (in the form of resting spores) is introduced at a point into a uniformly distributed population of uninfected larvae. The successive curves show the progress of the disease across the landscape at 1-wk intervals. This figure demonstrates first that the disease spreads slowly as it builds up in intensity near where it was introduced (Shigesada et al. 1995) but ultimately reaches higher spread rates. As the figure shows, in the first 1–3 wk, the spread of the disease is negligible; by the later weeks, however, the disease is spreading about 250 m each week. The second feature is that, once the disease reaches high infection rates near the point of introduction, it begins to travel across the landscape in an unchanging wave of infection, called a "traveling wave." To emphasize the time that it takes for the disease to form a traveling wave, in these simulations we introduced only a small number of resting spores, but the ultimate speed of the traveling wave is independent of the initial resting spores.

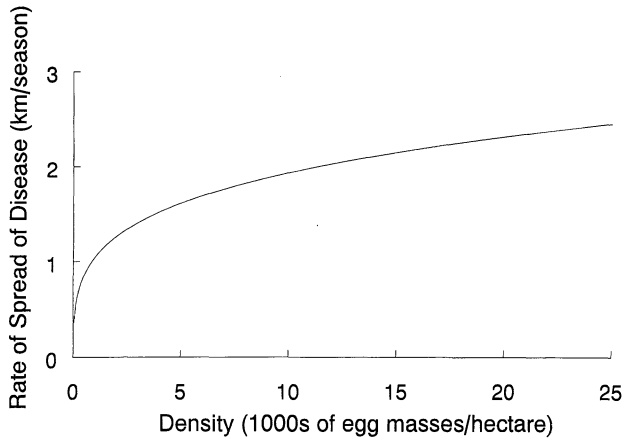


**Figure 3:** The model's prediction of the long-term rate of advance of a wavefront of *Entomophaga maimaiga,* plotted against gypsy moth density at the beginning of a season. The parameters here are again taken from the fit of the model to the Holloway Gap plot (fig. 2). Although the rate of advance at first increases rapidly with density, at the high gypsy moth densities typical of outbreak populations, density has little effect on the rate of advance of the wave, suggesting that we need only the roughest of estimates of density at the large scale to predict spread rates.

In the appendix we derive an expression for the rate at which the disease spreads spatially over the long term, and figure 3 demonstrates that this spread rate increases strongly with initial host density. Figures 1 and 3 thus form the basis for our hypothesis that the difference in the rate of spread of the disease at the two different spatial scales was due in part to differences in both host and pathogen density.

### *Fitting the Model to the Moderate Scale Data*

At the moderate scale of the experimental data, the disease spread no more than 300 m in a season, but at the large scale of the regional data, the disease spread more than 120 km in a season. The two data sets thus differ in spatial spread rate by a factor of about 400. The question

that we attempt to answer with the model is, What fraction of this discrepancy can be explained by the greater density of host and pathogen at the regional scale, where the disease had caused an intense epidemic in the preceding year? One of the useful features of the model is that it can be adapted to mimic spread at the two different scales. Our approach is, first, to fit the model to the moderate-scale experimental data; next, to use the resulting parameter values in the model to predict what the spread rate would be at the large scale of the regional data; and finally, to compare the observed and predicted rates of spread.

To simplify the fitting procedure, three of the model parameters were estimated independently of the moderate-scale data. The time between infection and death of infected larvae averages about 5.5 d, and the death rate of infected larvae $\alpha$ is the inverse of this average (Anderson and May 1981). The number of conidia produced by each larvae is $2 \times 10^5$ (Shimazu and Soper 1986), and the rate $\lambda$ at which larvae produce conidia is this number times the death rate $\alpha$ (Anderson and May 1981). Because the data demonstrate that humidity was sufficient to allow epidemics at both scales, it is likely that the rate of breakdown of conidia due to drying out was very slight (Hajek et al. 1990*b*). We therefore assume that the decay rate $\mu$ of the pathogen was close to 0 or about $10^{-6}$ $d^{-1}$. The initial density of egg masses was measured for each plot at the beginning of the season, and when multiplied by the number of eggs per mass (250) gives the overall density for each plot. To match the way that the data were collected, the model output is the cumulative fraction of larvae dead of the fungus by the end of the gypsy moth larval period. The remaining parameters that we need to estimate are the dispersal rate of conidia $D$, the conidial transmission rate $\nu_C$, and the force of infection of resting spores $\nu_R R$.

The statistical errors involved in fitting population data to mathematical models are typically classified as either process errors or observation errors (Dennis et al. 1995; Pascual and Kareiva 1996). Process errors quantify the discrepancy between the model and the data that occurs because the model does not accurately represent the biological mechanism that produced the data, while observation errors quantify the discrepancy that occurs because of error in the data. Although both errors usually occur simultaneously, partitioning the error in the fitting process into the fraction due to each type is typically not feasible (Pascual and Kareiva 1996), and many fitting efforts therefore concentrate on observation error. Nevertheless, both the transmission and dispersal of *E. maimaiga* conidia are sensitive to weather conditions, and the lack of weather data in our model means that the model oversimplifies the spread of the pathogen. Our approach was therefore to treat each fungal release plot as a realization of some underlying stochastic process, of which the model equations (1)–(3) are a deterministic representation. We first fit the model separately to each plot to generate values of the conidial transmission rate $\nu_C$, the conidial dispersal rate $D$, and the resting spore force of infection $\nu_R R$, under the assumption of binomial errors in the data. We then used the resulting nine best-fit values in the model to extrapolate to the large scale, first calculating a long-term spread rate from the parameters estimated for each plot, and then using bootstrapping to estimate the 95% confidence interval around the mean large-scale spread rate. In effect, we assumed that the differences among the plots are largely due to variability in weather conditions. By fitting the data to each plot under the assumption of binomial errors, we are assuming that the error in the model fit at the moderate scale is entirely due to observation error, but by using all nine plots together to estimate the confidence interval at a large scale, we are assuming that the error between the model fit and the large-scale data is due to process error.

Figure 2 shows the fit of the model to the data in each plot, demonstrating that the model in all cases provides an excellent fit to the moderate-scale data. Note that the fraction infected predicted by the model in the Piney River, Wiggins Springs, and Hunting Creek plots shows a steep spike near where the disease was introduced (the first 10 m on the horizontal axis). This effect occurs because of the effects of the resting spores by which the disease was introduced. That is, resting spores do not disperse and typically have high survival during the epidemic, so that when the resting spore force of infection is high relative to the transmission rate of conidia, then the fraction of larvae infected will be very high near where the disease was introduced.

### *Making Predictions at the Regional Scale*

For the regional data, we can use the long-term behavior of the model to sidestep our lack of detailed density information. As figure 1 shows, over the long term the model shows traveling waves that move with constant velocity, the shape and velocity of the wave do not depend on the initial introduction of the disease, and peak infection rates are nearly 100%. Infection rates in the epidemic that produced the regional spread data were typically in excess of 80% (Elkinton et al. 1991), suggesting that the regional spread may well have been due to a traveling wave of disease. Also, because the wave shape is unchanging, all parts of the wave move at the same speed, so the wave speed can be measured at any level of infection. This is important because presumably there is some minimum level of infection at which the fungus

can be detected. It does not matter what that minimum level is, as long as it did not vary too drastically between seasons.

To predict large-scale spread rates, we need the initial density of uninfected larvae at the regional scale. Because detailed density information is not available for such large areas, we instead use a likely value for outbreaking populations, which is about $2 \times 10^4$ egg masses $ha^{-1}$. In practice the precise value is of little importance because, at higher densities, the wave velocity is only mildly dependent on host density, as figure 3 shows.

In order to extrapolate from the moderate scale of the pathogen release plots to the large scale of regional spread, we used the parameters that we fit to each release plot to generate a large-scale spread rate (fig. 1), giving a mean spread rate of almost exactly 1 km $season^{-1}$. To estimate the 95% confidence interval around this mean spread rate, we bootstrapped the mean rate by randomly drawing, with replacement, 4,000 sets of nine samples from our nine velocities and calculating a mean velocity from each set of nine. The percentile method (Efron and Tibshirani 1993) then gave a 95% confidence interval of 0.52 to 1.52 km $season^{-1}$.

## Discussion

Fitting the model equations (1)–(3) to the experimental data in figure 2, and extrapolating to large scales (fig. 1), gives a mean regional scale spread rate that differs from the observed regional spread by a factor of about 120, and the confidence intervals of the two spread rates do not come close to overlapping. Clearly the large-scale spread rate of this disease cannot be explained in terms of spread at the moderate scale of the release experiment.

The question then becomes, What aspect of the biology of the spread of the disease is missing from the model? One simplification is that the model assumes that host density is uniform over space; it is likely, however, that including such variability would have the effect merely of causing the spread of the disease in the model to fluctuate correspondingly and so would not reduce the discrepancy between the model and the data. Although an increase in overall density in the model would decrease the discrepancy, making the model prediction at the large scale match the data would require unrealistically high densities.

We have also oversimplified the effects of moisture on the fungus. Both sporulation and conidial germination depend on moisture (Hajek et al. 1990*b*), and field experiments have shown that artificially increasing rainfall can increase disease in otherwise natural epidemics (Weseloh and Andreadis 1992). It is therefore possible that higher humidity at the regional level led to a higher spread rate than at the moderate scale. Nevertheless, an earlier simulation model of this host-pathogen system included most details of the influence of moisture, as well as a host of other factors (Hajek et al. 1993), yet rainfall explained only a relatively small fraction (0.27–0.37) of the variability in percentage infection in the model's output. Also, our procedure for estimating model parameters from the experimental data took into account natural variability in weather factors, in that differences in spread rates among plots were likely due to differences in weather conditions that included moisture. Our range of parameter estimates thus allowed for some weather-influenced variability in the model, yet even the tail of the distribution of the model's large-scale spread rates does not overlap the distribution of spread rates observed in nature (fitting the model to the pooled data from all nine plots gave a similar mean spread rate; G. Dwyer, unpublished simulations). We therefore suspect that including the effects of weather conditions would not substantially change our prediction of the spread rate of the pathogen at a large scale.

A more likely simplification underlying the discrepancy between model and data is the assumption that conidia obey the laws of diffusion. This is equivalent to assuming that the conidial dispersal curve is normal (or Gaussian; Okubo 1980), and changing this assumption may well lead to a reduced discrepancy between model and data. Models of population spread that allow for dispersal curves with tails longer (or "fatter," i.e., more platykurtic) than those of a normal curve show more rapid spread (van den Bosch et al. 1988; Kot et al. 1996), and long enough tails can lead to a spread rate that continuously accelerates with time. Changing the distribution of dispersal distances in the model would probably have very little effect on the fit of the model to the experimental release data but may lead to a more rapid spread at the larger scale. Although it seems unlikely that the increase in the rate of spread due to such a mechanism would be sufficient to eliminate the current two orders of magnitude discrepancy, clearly further exploration of such models is called for.

Our opinion, however, is that the missing detail in the model is long-distance conidial dispersal mechanisms that do not operate at smaller scales. Specifically, dispersal of conidia on wind currents above the forest canopy may play an important role in regional-scale dispersal. Ultimately, a useful understanding of the large-scale spread of this pathogen may require a model that combines our epidemiological approach with a more sophisticated treatment of the physics of wind currents and the structure of the air column. We caution, however, that more complicated models correspondingly require more detailed data, which are rarely available.

A related issue is that, in the model, the fungus does not jump ahead and form new foci of infection ahead of the wave of disease. Superficially it seems unlikely that this kind of effect would contribute much to the discrepancy between the predicted and observed large-scale spread rates. The resolution of the large-scale field data is not sufficient to demonstrate any such effects, however, so it is hard to know how important they are. Nevertheless, allowing for long-distance dispersal mechanisms may well lead to such an effect, so this is another argument for further development of the model.

Simple mathematical models in ecology have classically been viewed solely as qualitative tools, either in supplying general explanations for observed phenomena or in providing experimentally testable hypotheses. Here we have instead used a simple model as a quantitative tool for understanding data and, especially, for providing a link between data collected at different scales. The typical method of analyzing the kind of infection data that we show in figure 2 is to perform a linear regression of log-transformed mortality versus distance (Gregory 1968; Entwistle et al. 1983), but we hope to have demonstrated that a more mathematically sophisticated approach allows for comparison of different data sets and a more explicit consideration of mechanism. More biologically, our model prediction does reduce the discrepancy between the two data sets from a factor of 400 to a factor of 120, a reduction of some 70%. Although the remaining discrepancy is still huge, the reduction suggests that at least some of the difference between the spread rates at the two spatial scales was due to differences in density. In general, given the emphasis in the insect-pathogen literature on long-distance dispersal mechanisms (Young 1974; Entwistle et al. 1983), we think that it is useful to point out that, in fact, biological interactions can play an important quantitative role in population spatial spread. We emphasize that model simplicity per se is not the issue; instead, we strongly suspect that the model is missing only one or two key details. In fact, the simplicity of our model makes it easy to see that the model mechanism driving the more rapid rate of spread of the disease at the larger scale is due to higher densities of host and pathogen, and the small number of parameters in the model makes it much easier to assess the consequences of errors in parameter estimates (Ludwig et al. 1978; Ludwig and Walters 1985).

## APPENDIX

### Generating an Expression for the Rate of Spread of the Disease at a Large Scale

In this appendix, we present the details behind the wave speed calculation that was used to generate figure 3 and the long-term spread rates given in the main body of text. The analysis closely follows earlier work (Dwyer 1992; see also Murray et al. 1986). At the large spatial scale of the regional data set (Elkinton et al. 1991), the *Entomophaga maimaiga* epidemic probably approximated the traveling wave behavior seen in figure 1. Consequently the wave of infection rapidly moved beyond the area in which the resting spores, which began the epidemic, were found. Given that our interest is in the long-term behavior of the model, to match this behavior we therefore set $\nu_R = 0$ to make our prediction of long-term spread. The model is then:

$$\frac{\partial S}{\partial t} = -\nu_C CS; \tag{A1}$$

$$\frac{\partial I}{\partial t} = \nu_C CS - \alpha I; \tag{A2}$$

and

$$\frac{\partial C}{\partial t} = \lambda I - \mu C + D\frac{\partial^2 C}{\partial x^2}. \tag{A3}$$

The simulations in figure 1 show that solutions to the model form waves that travel with constant shape at a constant speed, so that the model can be converted to a moving coordinate system using the transformation $\xi = x + ct$. This converts the system of partial differential equations (A1)–(A3) to a system of ordinary differential equations:

$$cS' = -\nu CS; \tag{A4}$$

$$cI' = \nu CS - \alpha I; \tag{A5}$$

and

$$cC' = \lambda I - \mu C + DC''. \tag{A6}$$

To reduce this system of three second-order equations to a system of four first-order equations, we introduce the variable $y$ such that $C' = y$, so that we have

$$S' = -\frac{\nu}{c} CS; \tag{A7}$$

$$I' = \frac{\nu}{c} CS - \frac{\alpha}{c} I; \tag{A8}$$

$$C' = y \tag{A9}$$

and

$$y' = \frac{\lambda}{D} I - \frac{\mu}{D} C + \frac{c}{D} y. \tag{A10}$$

This set of differential equations has two nontrivial equilibria. The first is at $(S, I, C, y) = (S_0, 0, 0, 0)$, where $S_0$ is the initial value of $S$. The analysis requires that $S_0$ be

spatially uniform, although if we knew the spatial distribution of host densities at the regional scale, we could use simulations to generate a prediction.

The simulations show that traveling waves only develop if $S_0 > \alpha\mu/\nu\lambda$—in other words, only if the population exceeds some density threshold. For $S_0 > \alpha\mu/\nu\lambda$, equations (A7)–(A10) move from the spatially uniform equilibrium at $(S, I, C, y) = (S_0, 0, 0, 0, 0)$ to $(S, I, C, y) = (S_\infty, 0, 0, 0, 0)$, where $S_\infty$ is the density of hosts remaining after the epidemic has passed. We have not been able to generate an expression for $S_\infty$, but the simulations show that if $S_0$ is much bigger than $\alpha\mu/\nu\lambda$, $S_\infty$ is very small.

Given that the model shows traveling wave behavior, it is possible to calculate the minimum possible speed of the traveling wave using linear stability analysis of equations (A7)–(A10). Following the usual protocol gives an equation for the eigenvalues $\theta$ of the system linearized about $(S, I, C, y) = (S_0, 0, 0, 0, 0)$:

$$f(\theta) = \theta^3 + \left(\frac{\alpha}{c} - \frac{c}{D}\right)\theta^2 + \left(-\frac{\alpha}{D} - \frac{\mu}{D}\right)\theta + \frac{\nu\lambda S_0}{cD} - \frac{\alpha\mu}{cD}. \quad \text{(A11)}$$

The information that $f(0) > 0$, $f'(0) < 0$, and $f(\pm) = \pm\infty$ shows that $f(\theta)$ will have one negative real eigenvalue and a pair of complex conjugate eigenvalues. Sketching $f$ shows that, for sufficiently small $c$, the complex eigenvalues will have nonzero imaginary part, so that the system will oscillate in the vicinity of the equilibrium. Since at the equilibrium $I = C = 0$, this means that the population sizes $I$ and $C$ will sometimes be negative, which is biologically impossible. The minimum wave speed will therefore occur when $f(\theta)$ is tangent to the $\theta$ axis (so that all the eigenvalues are real). At this minimum $c_{\min}$, $\partial f/\partial\theta = 0$ and $f = 0$, so we can eliminate $\theta$ to find $c_{\min}$ in terms of the parameters of the model, including the initial host density $S_0$. From this procedure, we can find $c_{\min}$ as the positive root of $g(c_{\min}^2)$, where

$$g(z) = \frac{2}{27}\left(\frac{z^3}{D^3} - \frac{3\alpha z^2}{D^2} + \frac{3\alpha^2 z}{D^2} - \alpha^3\right) + \frac{1}{3}\left(\frac{\alpha z^2}{D^2} - \frac{\alpha^2 z}{D} + \frac{z^2\mu}{D^2} - \frac{\alpha\mu z}{D}\right) + \frac{2}{27}\left[\frac{z^2}{D^2} - 2\frac{\alpha z}{D} + \alpha^2 + 3z\left(\frac{\alpha}{D} + \frac{\alpha}{D}\right)\right]^{3/2} - \frac{\nu\lambda S_0 z}{D} + \frac{\mu\alpha z}{D}. \quad \text{(A12)}$$

It is clearly the case that $g(0) = 0$, and $\partial g/\partial z|_{z=0} < 0$ for $S_0 > \alpha\mu/\nu\lambda$, so that $g(z)$ has one positive real root. The square of this root is the minimum possible speed of the traveling wave. Although proving that the model waves necessarily travel at this speed is exceedingly difficult, waves in the simulations travel at the minimum speed, strongly suggesting that it is the most stable. Also, the speed of waves in simulations of the unmodified model equations (1)–(3) matches this speed, confirming that the modified model equations (A1)–(A3) are an accurate approximation to equations (1)–(3). Moreover, the minimum speed has similarly been observed to be the most stable for a variety of similar models (Murray et al. 1986; Mollison 1991).

For $S_0 > \alpha\mu/\nu\lambda$ and $c$ not too small, $f(\theta)$ has two (identical) eigenvalues with positive real parts and one with a negative real part. For $S_0 < \alpha\mu/\nu\lambda$ there will instead be one eigenvalue with a positive real part and two with negative real parts. An important point is that here the independent variable $\xi$ is not the same as time $t$ but is instead $x + ct$. This means that the signs on the real parts of the eigenvalues do not indicate stability in the usual sense (whether or not the populations will reach an equilibrium) but, rather, the direction of flow in the vicinity of equilibria. This is because the direction of positive $\xi$ is arbitrary, indicating only the direction (right or left) of the advance of the wave. Nevertheless, the fact that there is one negative and two positive real parts for the eigenvalues for the equilibrium at which $S_0 > \alpha\mu/\nu\lambda$, and one positive and two negative real parts for the eigenvalues for the equilibrium at which $S_0 < \alpha\mu/\nu\lambda$ indicates that it is at least topologically possible for a trajectory to leave an equilibrium at $(S_0 > \alpha\mu/\nu\lambda, 0, 0, 0)$ and arrive at an equilibrium at $(S_0 < \alpha\mu/\nu\lambda, 0, 0, 0)$. The simulations demonstrate that such trajectories do exist.

The final step is to demonstrate that there is no trajectory from $(S_0, 0, 0, 0)$ to the origin $(0, 0, 0, 0)$. The eigenvalues of the system linearized about the origin are

$$\theta = 0, -\frac{\alpha}{c}, \frac{c}{2D} \pm \frac{1}{2}\sqrt{\left(\frac{c}{D}\right)^2 + \frac{4\mu}{D}}. \quad \text{(A13)}$$

In the vicinity of the origin, the trajectories that approach the origin will be governed by the solutions with negative eigenvalues, that is, by

$$\theta = -\frac{\alpha}{c}, -\frac{1}{2}\sqrt{\left(\frac{c}{D}\right)^2 + \frac{4\mu}{D}}. \quad \text{(A14)}$$

The eigenvectors associated with these eigenvalues are $(0, A, B, C, D)^T$ and $(0, 0, 0, 0)^T$, respectively. In other words, trajectories that approach the origin do so in the $S = 0$ subspace. Replacing $\xi$ by $-\xi$ in equations (A7)–(A10) shows that if $S = 0$, then it has always been 0.

Consequently, any trajectory leaving ($S_0$, 0, 0, 0) will never reach the origin.

## Literature Cited


Anderson, R. M., and R. M. May. 1981. The population dynamics of microparasites and their invertebrate hosts. Philosophical Transactions of the Royal Society of London B, Biological Sciences 291:451–524.

———. 1994. Infectious diseases of humans: dynamics and control. Oxford University Press, Oxford.

Campbell, R. W. 1981. Population dynamics. Pages 161–202 *in* C. C. Doane and M. L. McManus, eds. The gypsy moth: research toward integrated pest management. USDA Technical Bulletin 1584. U.S. Department of Agriculture, Washington, D.C.

Dennis, B., R. A. Desharnais, J. M. Cushing, and R. F. Constantino. 1995. Nonlinear demographic dynamics: mathematical models, statistical methods, and biological experiments. Ecological Monographs 65:261–282.

Dwyer, G. 1992. On the spatial spread of insect pathogens: theory and experiment. Ecology 73:479–494.

Efron, B., and R. J. Tibshirani. 1993. An introduction to the bootstrap. Chapman & Hall, New York.

Elkinton, J. S., and A. M. Liebhold. 1990. Population dynamics of gypsy moth in North America. Annual Review of Entomology 35:571–596.

Elkinton, J. S., A. E. Hajek, G. H. Boettner, and E. E. Simons. 1991. Distribution and apparent spread of *Entomophaga maimaiga* (Zygomycetes: Entomphthorales) in gypsy moth (Lepidoptera: Lymantriidae) populations in North America. Environmental Entomology 20:1601–1605.

Entwistle, P. F., P. H. W. Adams, H. F. Evans, and C. F. Rivers. 1983. Epizootiology of a nuclear polyhedrosis virus (baculoviridae) in European spruce sawfly *Gilpinia hercyniae:* spread of disease from small epicentres in comparison with spread of baculovirus diseases in other hosts. Journal of Applied Ecology 20:473–487.

Fuxa, J. R., and Y. Tanada. 1987. Epidemiological concepts applied to insect epizootiology. Pages 43–68 *in* J. R. Fuxa and Y. Tanada, eds. Epizootiology of insect diseases. Wiley, New York.

Gregory, P. H. 1968. Interpreting plant disease gradients. Annual Review of Phytopathology 6:189–212.

Gypsy Moth News. 1990. Gypsy Moth News, no. 24. USDA Forest Service, Morgantown, W.V.

Hajek, A. E., R. A. Humber, J. S. Elkinton, B. May, S. R. A. Walsh, and J. C. Silver. 1990*a*. Allozyme and RFLP analyses confirm *Entomophaga maimaiga* responsible for 1989 epizootics in North American gypsy moth populations. Proceedings of the National Academy of Sciences of the USA 87:6979–6982.

Hajek, A. E., R. I. Carruthers, and R. S. Soper. 1990*b*. Temperature and moisture relations of sporulation and germination by *Entomophaga maimaiga* (Zygomycetes: Entomophthorales), a fungal pathogen of *Lymantriadispar* (Lepidoptera: Lymantriidae). Environmental Entomology 19:85–90.

Hajek, A. E., T. S. Larkin, R. I. Carruthers, and R. S. Silver. 1993. Modelling the dynamics of *Entomophaga maimaiga* (Zygomycetes: Entomophorales) epizootics in gypsy moth (Lepidoptera: Lymantriidae) populations. Environmental Entomology 22:1172–1187.

Hajek, A. E., R. A. Humber, and J. S. Elkinton. 1995. The mysterious origin of *Entomophaga maimaiga* in North America. American Entomologist 41:31–42.

Hajek, A. E., J. S. Elkinton, and J. J. Witcosky. 1996. Introduction and spread of the fungal pathogen *Entomophaga maimaiga* along the leading edge of gypsy moth spread. Environmental Entomology 25:1235–1247.

Kareiva, P., and M. Andersen. 1990. Spatial aspects of population interactions: the wedding of models and experiments. Pages 33–50 *in* J. Roughgarden, R. M. May, and S. A. Levin, eds. Perspectives in ecological theory. Princeton University Press, Princeton, N.J.

Kot, M., M. A. Lewis, and P. van den Driessche. 1996. Dispersal data and the spread of invading organisms. Ecology 77:2027–2042.

Liebhold, A. M., J. S. Elkinton, and W. E. Wallner. 1986. Effect of burlap bands on between-tree movement of late-instar gypsy moth, *Lymantria dispar* (Lep: Lymantriidae). Environmental Entomology 15:373–379.

Ludwig, D., and C. Walters. 1985. Are age-structured models appropriate for catch-effort data? Canadian Journal of Fisheries and Aquatic Science 42:1066–1072.

Ludwig, D., D. D. Jones, and C. S. Holling. 1978. Qualitative analysis of insect outbreak systems: the spruce budworm and forest. Journal of Animal Ecology 47: 315–332.

Mollison, D. 1991. Dependence of epidemic and population velocities on basic parameters. Mathematical Biosciences 107:255–287.

Mooney, H. A., and J. A. Drake. 1986. Ecology of biological invasions of North America and Hawaii. Springer, New York.

Murray, J. D. 1989. Mathematical biology. Springer, New York.

Murray, J. D., E. A. Stanley, and D. L. Brown. 1986. On the spatial spread of rabies among foxes. Proceedings of the Royal Society of London B, Biological Sciences 229:111–150.

Okubo, A. 1980. Diffusion and ecological problems: mathematical models. Springer, New York.

Okubo, A., and S. A. Levin. 1989. A theoretical frame-

work for data analysis of wind dispersal of seeds and pollen. Ecology 70:329–338.

Pascual, M. A., and P. Kareiva. 1996. Predicting the outcome of competition using experimental data: maximum likelihood and Bayesian approaches. Ecology 77: 337–349.

Pasquill, F., and F. B. Smith. 1983. Atmospheric diffusion. 3d ed. Halsted, New York.

Shigesada, N., K. Kawasaki, and Y. Takeda. 1995. Modeling stratified diffusion in biological invasions. American Naturalist 146:229–251.

Shimazu, M., and R. S. Soper. 1986. Pathogenicity and sporulation of *Entomophaga maimaiga* Humber, Shimazu et Soper (Entomophthorales: Entomophthoraceae). Applied Entomology and Zoology 21:589–596.

Tanada, Y., and H. K. Kaya. 1993. Insect pathology. Academic Press, San Diego, Calif.

van den Bosch, F., J. C. Zadoks, and J. A. J. Metz. 1988. Focus expansion in plant disease. III. Two experimental examples. Phytopathology 78:919–925.

Vitousek, P. M. 1994. Beyond global warming: ecology and global change. Ecology 75:1861.

Weseloh, R., and T. G. Andreadis. 1992. Epizootiology of the fungus *Entomophaga maimaiga,* and its impact on gypsy moth populations. Journal of Invertebrate Populations 59:133–141.

Woods, S., J. S. Elkinton, K. D. Murray, A. M. Liebhold, J. R. Gould, and J. D. Podgwaite. 1991. Transmission dynamics of a nuclear polyhedrosis virus and predicting mortality in gypsy moth (Lepidoptera: Lymantriidae) populations. Journal of Economic Entomology 84:423–430.

Young, E. C. 1974. The epizootiology of two pathogens of the coconut palm rhinoceros beetle. Journal of Invertebrate Pathology 24:82–92.

Associate Editor: Bryan T. Grenfell